JOURNAL OF GEOPHYSICAL RESEARCH, VOL. 112, A06326, doi:10.1029/2006JA011625, 2007

Effects of the ionosphere and solar activity on radio occultation signals: Application to CHAllenging Minisatellite Payload satellite observations

A. G. Pavelyev,[1] Y. A. Liou,[2,5] J. Wickert,[3] T. Schmidt,[3] A. A. Pavelyev,[1] and S. F. Liu[4]

Received 23 January 2006; revised 29 November 2006; accepted 27 February 2007; published 28 June 2007.

[1] We analyze the ionospheric effect on the phase and amplitude of radio occultation (RO) signal. The introduced theoretical model predicts a correlation between the phase acceleration and intensity variations of RO signal and opens a way to locate layered structures in the propagation medium, in particular, in trans-ionospheric satellite-to-satellite links. For considered CHAllenging Minisatellite Payload (CHAMP) RO events, the locations of the inclined plasma layers in the lower ionosphere are estimated, and the electron density distribution is retrieved. By analysis of the CHAMP RO data, we reveal the dependence of the intensity variations of RO signal on sharp changes in the *DST* index and on the local time. Maps of the seasonal, geographical, and temporal distributions of the CHAMP RO events with amplitude scintillations, having high S_4 index values, and observed during the years 2001–2004 indicate dependence on solar activity. As follows from this analysis, the GPS signals in the trans-ionospheric links can be used for investigating the location and parameters of inclined plasma layers and monitoring the influence of solar activity on the ionosphere with global coverage.

Citation: Pavelyev, A. G., Y. A. Liou, J. Wickert, T. Schmidt, A. A. Pavelyev, and S. F. Liu (2007), Effects of the ionosphere and solar activity on radio occultation signals: Application to CHAllenging Minisatellite Payload satellite observations, *J. Geophys. Res.*, *112*, A06326, doi:10.1029/2006JA011625.

1. Introduction

[2] The origin of sporadic plasma structures in the near-Earth space are related to wave activity in the ionosphere, and mesosphere, effects of variations in the ionizing solar radiation at different wavelengths, and solar wind interaction with the Earth's magnetosphere [e.g., *Yizengaw et al.*, 2005]. Localization and estimation of the electron density distribution in the plasma disturbances in the ionosphere have been done previously by tomographic and radio-holographic methods by use of the radio signals in trans-ionospheric satellite-to-Earth links [*Kunitsyn and Tereshchenko*, 2003, and references therein]. The phase variations during propagation of the high-accuracy Global Positioning satellite System (GPS) signals make it possible to sound the topside ionosphere/plasmasphere on the basis of measurements from the Low Earth Orbiter (LEO) satellites [*Heise et al.*, 2002]. Therefore the GPS/GLONASS satellite navigational systems with more than 50 satellites, which are located in circular orbits with an inclination of about 70 and a height of ~20,000 km above the ground surface and emit at wavelengths of 19 and 24 cm, makes it possible to globally observe the processes in the Earth's plasma sheath above the LEO satellite [*Yizengaw et al.*, 2005, 2006].

[3] The radio signals emitted by GPS at two carrier frequencies (f_1 = 1575.42 MHz and f_2 = 1227.6 MHz) are currently used in radio occultation (RO) studies of the *F* and *E* layers below the LEO satellite [*Hajj and Romans*, 1998; *Schreiner et al.*, 1999; *Vorob'ev et al.*, 1999, *Wickert et al.*, 2001; *Gorbunov et al.*, 2002; *Sokolovskiy et al.*, 2002], and especially sporadic *E* layers of the ionosphere [*Igarashi et al.*, 2001, 2002; *Hocke et al.*, 2001, 2002; *Pavelyev et al.*, 2002, 2003; *Wickert et al.*, 2004a; *Wu et al.*, 2005]. These investigations are concentrated on the ionospheric influence on highly precise GPS radio signals [*Pavelyev et al.*, 2005a, 2005b; *Liou et al.*, 2005], and on the determination of the vertical distribution of electron density in the lower ionosphere as function of altitude [*Igarashi et al.*, 2001, 2002; *Hocke et al.*, 2001, 2002; *Pavelyev et al.*, 2002, 2003; *Wickert et al.*, 2004a]. The information on the electron density distribution in the lower ionosphere is an important source for estimation of the off-equatorial height-integrated conductivity [*Kelley et al.*, 2004]. All these investigations are important for modernization of the published information on the morphology of the ionosphere and ionospheric processes [*Kelley*, 1989].

[1]Institute of Radio Engineering and Electronics, Russian Academy of Sciences, Moscow region, Russia.
[2]Center for Space and Remote Sensing Research, National Central University, Chung-Li, Taiwan.
[3]GeoForschungsZentrum Potsdam, Potsdam, Germany.
[4]Department of Industrial Design, National Cheng Kung University, Tainan, Taiwan.
[5]Also with College of Electrical Engineering and Computer Science, Chin Yun University, Chung-Li, Taiwan.

0148-0227/07/2006JA011625$09.00

[4] The RO technique differs significantly as compared to ionospheric tomography methods. The RO sounding is fulfilled from nearly constant direction in contrast with tomographic methods, which sound the propagation medium from significantly different directions [*Kunitsyn and Tereshchenko*, 2003]. In essence, the RO technique is designed for investigation of the layered structures in a spherical symmetric propagation medium. The electron density, found under the assumption of the spherical symmetry, is assigned to the ray perigee T on a ray trajectory GTL connecting the GPS and LEO satellites [*Hajj et al.*, 2002]. At GPS frequencies, point T practically coincides with projection Q of the center of spherical symmetry O on the line of sight GQL (Figure 1). In general, the assumption of the spherical symmetry cannot be applied directly to locate sporadic ionospheric disturbances [*Wickert et al.*, 2004a; *Pavelyev et al.*, 2005a; *Liou et al.*, 2005].

[5] The investigations provided by *Wu et al.* [2005], *Wickert et al.* [2004b], and *Pavelyev et al.* [2005b] showed that the reasonable global morphology and occurrence of plasma disturbances and sporadic E_s layers in the ionosphere may be produced on a monthly and seasonal basis by analysis of the phase and amplitude variations of the CHAMP RO signal. However, it is unclear up until now how to estimate the location of the plasma layers in the lower ionosphere by the RO method [*Wickert et al.*, 2004a]. Apparently, a possibility of the RO method to locate the plasma disturbances depends on their type.

[6] *Gorbunov et al.* [2002] and *Sokolovskiy et al.* [2002] applied the back propagation radio-holographic method to locate ionospheric disturbances in the E and F layer of the ionosphere by use of RO data analysis. *Wickert et al.* [2004a] introduced a new approach to determine the distribution of the electron density in sporadic plasma structures in the ionosphere. This approach is based on the assumption of an inclined plasma layer. *Wickert et al.* [2004b] indicated a difficulty in locating an inclined plasma layer and resolving uncertainty in its location between the parts GT and TL of the ray trajectory GTL (Figure 1).

[7] In this paper we introduce a new method of locating the sporadic layered structures in the ionosphere and establishing the origin of the RO signal scintillations observed at the mesospheric and stratospheric altitudes of the ray perigee in the trans-ionospheric satellite-satellite link. We demonstrate also a relation between solar activity and variations in RO signal intensity by use of the CHAMP RO data.

2. RO Method for Measuring Parameters of the Near-Earth Propagation Medium

[8] The scheme of the radio occultation experiment in trans-ionospheric satellite-to-satellite link is shown in Figure 1. Radio waves emitted by the GPS satellite (point G) arrive at a receiver onboard the LEO satellite (point L) along the ray GTL, where T is the ray perigee. At point T, the ray's distance from the Earth's surface h is minimal. The projection of point T on the Earth's surface determines the coordinates of the RO region, latitude φ and longitude λ_l. Point O (Figure 1) is the center of the spherical symmetric distribution of the refractivity $N(h)$ in the Earth's atmosphere and ionosphere. Point O coincides with the local

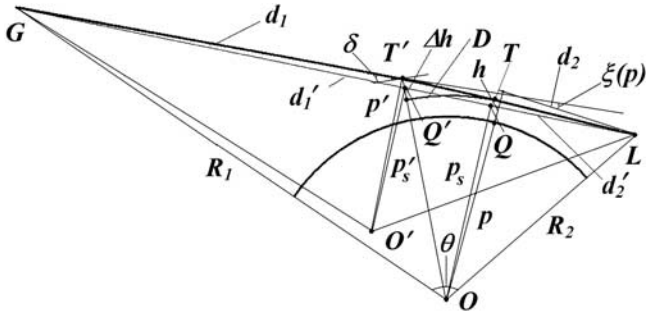

Figure 1. Scheme of trans-ionospheric satellite-to-satellite link.

center of curvature of the Earth's surface (ellipsoid) in the plane LGO (Figure 1) [*Hajj et al.*, 2002]. In the case of spherical symmetry, the ray perigee T coincides with position of tangent point, where gradient of refractivity $N(h)$ is perpendicular to the ray trajectory GTL (Figure 1). Record of the RO signal $E(t)$ along the LEO trajectory at two GPS frequencies f_1 = 1575.42 MHz and f_2 = 1227.6 MHz contains the amplitudes $A_1(t)$ and $A_2(t)$, respectively, along the phase path excesses $\Phi_1(t)$ and $\Phi_2(t)$ of the radio field as functions of time.

[9] The vertical velocity of the occultation beam path $v_\perp$ is usually about 2 km/s in the RO experiments. This value of $v_\perp$ is many times greater than those corresponding to the motion of layers in the ionosphere and atmosphere. Therefore the satellite radio-holograms contain quasi-instantaneous image of the Earth environment in the RO region. The phase variations of the RO signal can be applied to determine the impact parameter p of the ray trajectory GTL and the bending angle $\xi(p)$ (Figure 1) by use of known satellite trajectory data [*Hajj et al.*, 2002]. Then, the electron density $N_e(p)$ in the ionosphere and the vertical profiles of refractivity $N(p)$ in the neutral atmosphere can be determined by different methods based on the Abel transform [*Steiner et al.*, 1999; *Hocke et al.*, 2001; *Pavelyev et al.*, 2002, 2003; *Igarashi et al.*, 2002]. The altitude h of the ray perigee T can be determined from the known values of the Earth curvature radius a_e, impact parameter p, and refractivity $N(p)$ under assumption of spherical symmetry with the center at point O [*Hajj et al.*, 2002]. The amplitude variations of the RO signals are also used to determine the vertical gradient of the refractivity $dN(h) / dh$ and electron density $dNe(h) / dh$ [*Igarashi et al.*, 2002; *Liou et al.*, 2002]. Note that at GPS frequencies, the refractivity is small and the location of the point T in the upper atmosphere and ionosphere practically coincides with the projection of the center of spherical symmetry O on the line of sight direction GL, point Q (Figure 1). Therefore, in the upper atmosphere and ionosphere, the height h of the ray perigee T can be calculated directly by use of a known location of the spherical symmetry center O and trajectory data.

[10] Horizontal gradients in the neutral atmosphere and plasma disturbances in the ionosphere can cause additional variations in the amplitude and phase of the RO signal and change the location of the center of spherical symmetry [*Wickert et al.*, 2004a]. As a consequence, one can observe significant variations of the amplitude and phase of the RO signals in the 40- to 80-km altitude interval of the ray

perigee T, in which the expected contributions from the neutral gas or the electron density in the RO signal changes are negligible at both GPS frequencies [*Sokolovskiy et al.*, 2002; *Wu et al.*, 2005]. *Wickert et al* [2004a] introduced a hypothesis that the origin of intense variations in RO signal in this altitude interval of the ray perigee T can be related to the influence of inclined layered structures, which displaces the tangent point along a ray trajectory GTL (Figure 1) to a new position T'. The new location of the tangent point (Figure 1) can appear owing to regular horizontal gradients in the ionospheric E and F regions and, possibly, in the lower magnetosphere. At a new tangent point T', located at a distance D relative to the ray perigee T, the intense refractivity gradient in the inclined layered structure is perpendicular to the ray GTL, and the height h is changed by magnitude $\Delta h = D^2 / r$, where r is the distance OT [*Wickert et al.*, 2004a] (Figure 1). The sign of the horizontal displacement D is positive when the point T' is located between T and G and is negative in the opposite case, when T' is located between T and L (Figure 1). The elevation angle δ of the inclined structure relative to the local horizontal direction is equal to $\delta = D / r$ (Figure 1).

[11] Radio wave propagation in the inclined layered structures can be described by a model of locally spherical symmetric layer [*Pavelyev et al.*, 1996], which relates the amplitude and phase variations in different sections of a raypath of the RO signal with parameters of the near-Earth medium. According to this model, the phase path of the radio waves is more sensitive to long-scale variations in refractivity, whereas the amplitude is sensitive to the refractivity gradients at the tangent points on the RO signal trajectory. Despite the dependence on noise of a receiver and receiving antenna and variations in the emitted power and antennas gain, the RO signal amplitude is a valuable source of information about characteristics of the near-Earth medium [*Sokolovskiy et al.*, 2002; *Liou et al.*, 2002].

[12] To establish the origin of the amplitude scintillations in the 40- to 80-km height interval of point T, it is necessary to analyze the connections between the phase and amplitude variations of the RO signal. The radio-physical model of the locally spherical symmetric layer permits one to obtain an important connection between the phase and amplitude variations of the radio wave propagating through a layered medium [*Pavelyev et al.*, 1996, 1997, 2004]. To establish this connection, we will use the relations obtained formerly [*Pavelyev et al.*, 2002, 2004; *Liou et al.*, 2006] between the phase-path excess $\Phi(p)$ and the refraction attenuation X of the radio waves propagating in a spherical symmetric medium with the center of symmetry located in point O (Figure 1)

$$\Phi(p) = L(p) + \kappa(p) - R_0 \tag{1}$$

$$X(p) = pR_0^2\left[R_1R_2d_1d_2\sin\theta\left|\partial\theta/\partial p\right|\right]^{-1} \tag{2}$$

$$\partial\theta/\partial p = \mathrm{d}\xi/\mathrm{d}p - (1/d_1 + 1/d_2) \tag{3}$$

where $\kappa(p)$is the main refractivity part of the phase path excess, $\xi(p) = -\mathrm{d}\kappa(p) / \mathrm{d}p$ is the refraction angle, $\theta(p)$ is the central angle, p, p_s are the impact parameter of the ray trajectory GTL and the line of sight GQL, respectively, R_0, R_1, R_2 are the distances GL, OG, and OL, correspondingly, $L(p)$ is the distance GTL, and d_1, d_2 are two short lengths, GT and TL, which are approximately equal to GQ and QL (Figure 1). Under condition

$$|p - p_s| << p_s \tag{4}$$

the derivative $\mathrm{d}\Phi(p) / \mathrm{d}t$sis equal to (*Liou et al.*, 2005):

$$\mathrm{d}\Phi(p)/\mathrm{d}t \approx (p - p_s)\partial\theta/\partial p_s \tag{5}$$

$$\partial\theta/\partial p_s = -(1/d_{1s} + 1/d_{2s}) \tag{6}$$

where d_{1s} and d_{2s} are the distances GQ and QL, respectively (Figure 1). The second derivative $\Phi(p)$ on time can be obtained from equation (5) under condition:

$$|(p - p_s)\mathrm{d}(\partial\theta/\partial p_s)/\mathrm{d}t| << |(\mathrm{d}p/\mathrm{d}t - \mathrm{d}p_s/\mathrm{d}t)\partial\theta/\partial p_s| \tag{7}$$

$$\mathrm{d}^2\Phi(p)/\mathrm{d}t^2 \approx \left(\mathrm{d}p/\mathrm{d}t - \mathrm{d}p_s/\mathrm{d}t\right)\mathrm{d}p_s/\mathrm{d}t\partial\theta/\partial p_s \tag{8}$$

Condition (7), in essence, is equivalent to inequality $|(p - p_s) / (R_2^2 - p^2)^{1/2}| \ll |X - 1|$, which is valid because the magnitude of its left part, $|(p - p_s) / (R_2^2 - p^2)^{1/2}|$, in the ionosphere, where variations in $|(p - p_s)|$ are about 0.01–0.1 km, is usually well below the amplitude of regular variations in $|X - 1| \sim 0.05 - 0.8$, and is comparable with the relative intensity of noise in radio occultation signal $\sim 10^{-5}$. By use of equation $\mathrm{d}p / \mathrm{d}t - \mathrm{d}p_s/\mathrm{d}t = [X(t) - 1]\,\mathrm{d}p_s / \mathrm{d}t$ [*Liou et al.*, 2006], one can obtain from equations (6) and (8):

$$1 - X(t) = ma, \qquad a = \mathrm{d}^2\Phi(t)/\mathrm{d}t^2 \tag{9}$$

$$m = q/(\mathrm{d}p_s/\mathrm{d}t)^2 \tag{10}$$

$$q = d_1d_2/(d_1 + d_2), \qquad d_1 + d_2 = R_0 \tag{11}$$

[13] Equation (9) indicates equivalence between the variations of the phase path excess acceleration $a = \mathrm{d}^2\Phi(t) / \mathrm{d}t^2$ and refraction attenuation $X(t)$. Usually, during the RO experiments, parameters m and $\mathrm{d}p_s / \mathrm{d}t$ are known from the orbital data because the location of the spherical symmetry center O and its projection on the line of sight, point Q are known and the distance GT d_1 and TL d_2 can be easily estimated as $d_{1,2} = (R_{1,2}^2 - p^2)^{1/2}$ (Figure 1). Therefore equation (6) gives a possibility to recalculate the phase acceleration a to the refraction attenuation X for the case when the center of spherical symmetry coincides with point O (Figure 1). This is useful for excluding the systematic errors from the phase and/or amplitude data. This is also useful for the estimation of the absorption of radio waves along the raypath GTL (Figure 1). The refraction attenuation X_e is determined from the amplitude data as a ratio of intensity of radio signal propagating through the atmosphere

to its intensity in free space. Thus, the experimental value X_e contains both the refraction and absorption effect. However, the phase acceleration depends on the refraction effect only. This gives a possibility to determine the absorption along the raypath *GTL* $Y(t)$ as a ratio:

$$Y(t) = X_e(t)/(1 - ma) \tag{12}$$

[14] This possibility should be investigated in detail because its importance for RO occultation measurements of the water vapor and minor atmospheric gas constituents in the atmosphere. The difficulty of RO technology consists of removing the refraction attenuation effect from the amplitude data. Equation (12) indicates the feasible way to solve this problem. However, the detailed analysis of the methodology is beyond the scope of this paper and will be considered in the future publications.

[15] At the GPS frequencies, the absorption effect caused by the ionosphere is small, and equations (9), (10), and (11) are useful to control the deflections from the spherical symmetry.

[16] The horizontal gradients in the ionosphere and atmosphere can displace the tangent point T along the ray trajectory to point T' because of deflection of the center of the spherical symmetry from its standard position, point O to point O' (Figure 1). As a consequence, the value of distance $T'L$ [approximately equal to LQ' (Figure 1)] will change to $d_2{}'$ and parameter m will also change its magnitude. However, equations (6), (7), and (8) are valid in the case of local spherical symmetry with new center O'. Therefore if the magnitude of parameter m will be estimated from the experimental data, it is possible to find new value of distance $T'L$ $d_2{}'$. For determination of the parameter m from the experimental data, we can assume that the value m is a slowly changing function of time. If noise is very small, parameter m can be determined directly from equation (6) as a ratio:

$$m = [1 - X(t)]/a. \tag{13}$$

[17] In the presence of noise, the value $m(t_k)$ can be determined approximately as a ratio of average of the squared refraction attenuation and phase acceleration variations:

$$m(t_k) = \left\{ \sum_{i=k-M}^{i=k+m} [X(t_i) - 1]^2 \Big/ \sum_{i=k-M}^{i=k+M} [a(t_i)]^2 \right\}^{1/2}, \tag{14}$$

where $2M$ is a number of samples for averaging, and $X(t_i)$, $a(t_i)$ are the current values of the refraction attenuation and phase acceleration variations, respectively, at the time instant t_i. Equation (14) is valid if the time interval for averaging is far below the time scale of changes of magnitude m, and there is a complete correlation between the refraction attenuation and the phase acceleration according to equation (9). In real conditions, there are different sources of amplitude and phase variations of the RO signal (for example, turbulence, multipath propagation, etc.), which do not obey equation (9). However, the amplitude and phase variations corresponding to inclined layered structures in the atmosphere and ionosphere must obey relationship (9), and parameter m can be determined in addition to equations (13) and (14) as a correlation coefficient between the refraction attenuation $X(t_i) - 1$ and the phase acceleration $a(t_i)$:

$$m(t_k) = \sum_{i=k-M}^{i=k+M} [1 - X(t_i)]a(t_i) \Big/ \sum_{i=k-M}^{i=k+M} [a(t_i)]^2 \tag{15}$$

[18] Equation (14) and (15) give the upper and lower boundary of parameter m, respectively. Then, after use of equations (9) and (10), one can estimate the upper and lower boundaries of the distance $D = d_2{}' - d_2 = d_2{}' - (R_2^2 - p^2)^{1/2}$. In the case of a full correlation between the refraction attenuation and phase acceleration, the influence of the layered structures prevails, the upper and lower boundaries are coinciding, and parameter m and displacement D can be evaluated exactly. At altitudes above 35 km both the numerator and denominators in equations (13), (14) and (15) may be small, which make determination of parameter m susceptible to measurements errors. However, in the case of sharp gradients in sporadic layered ionospheric structures, the amplitude and phase scintillations in the RO signal may be large enough to achieve necessary accuracy.

[19] Note that one must account for the velocity of the point O' in relations (9) and (10). In the case of the Earth atmosphere and ionosphere, the velocities of motion of layers and point O' are small as compared to the orbital velocities of the GPS and LEO satellites.

3. Origin of the Amplitude and Phase Variation in CHAMP RO Signals

[20] A description of the CHAMP RO mission is given by various publications [e.g., *Wickert et al.*, 2001]. The data archives used in this work may be accessed at http://isdc.gfz-potsdam.de/champ. Results of CHAMP RO measurement of the phase and amplitude of the GPS signals are shown in Figure 2 for RO event no. 0001, 21 September 2003, at 13 h 21 min local time with geographical coordinate 83.4S latitude and 161.8W longitude. The height h of ray perigee evaluated from orbital data by use of a standard model of refractivity $N(h) = N_0\exp(-h / H)$ in the Earth atmosphere, where N_0 is refractivity at the Earth surface, and $H \approx 6.3$ km is the height scale, is depicted on the horizontal axis in Figure 2. The plotted points correspond to sampling frequency 50 Hz. The height-sampling interval is about 30 m, depending on the vertical RO beam velocity. Curves 1 and 2 indicate results of measurements of the phase path excesses at two GPS frequencies F2 and F1, respectively (Figure 2, left panel). For a better comparison, the phase path excess calculated by use of the refractivity model [*Pavelyev et al.*, 1996] has been subtracted from the phase path excesses F1, F2, and F0 (curves 1–3 in Figure 2, left panel). All data in Figure 2 correspond to the altitudes retrieved by use of the Abel-inverted refractivity. The phase path excess residual F0 (curve 3, Figure 2, left panel) has been obtained after ionospheric correction, i.e., after excluding the ionospheric influence by linear combination of the phase path excesses residuals at the frequencies F1 and F2. The phase residuals corresponding to the neutral gas (curve 3 in Figure 2, left panel) are changing from -1 m at the 30-km altitude to -8 m at the 5-km altitude. These values correspond to a distinction of the vertical profile of

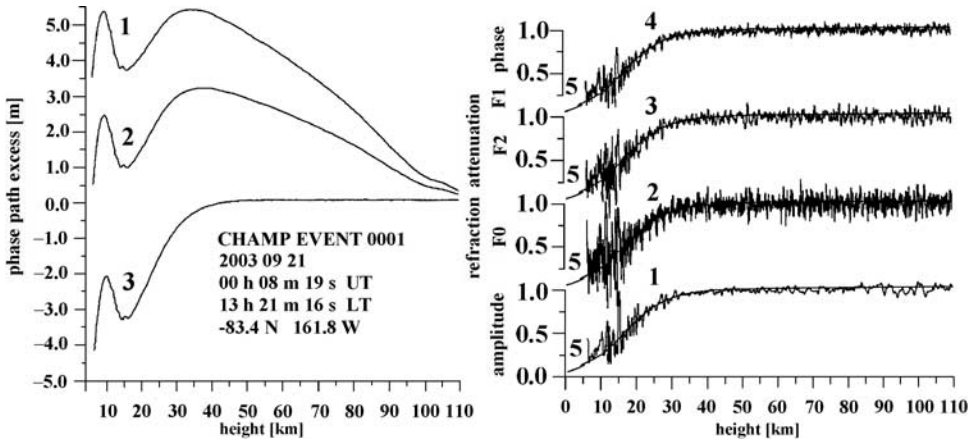

Figure 2. An example of CHAMP measurements. Left panel, the phase path excess residuals F1 and F2 as functions of height retrieved by use of the Abel-inverted refractivity (curves 1 and 2, respectively). The phase path excess residuals F1, F2 and F0 have been calculated by subtracting the phase excess evaluated by use of the refractivity model of the neutral atmosphere from the measured phase excesses F1 and F2. The phase path excess residual F0 (curve 3) has been obtained after ionospheric correction, i.e., after excluding the ionospheric influence by a linear combination of the phase path excesses residuals at the frequencies F1 and F2. Right panel, the refraction attenuation of the radio waves (curves 1–4) obtained from the amplitude (curve 1) and phase (curves 2–4) data as functions of height retrieved by use of the Abel-inverted refractivity. Smooth curves 5 indicate result of modeling of the refraction attenuation by use of the refractivity model of the neutral atmosphere.

refractivity in the polar atmosphere from the altitude profile of the refractivity used for simulation of the phase excess. Curve 1 in Figure 2, right panel, demonstrates the refraction attenuation variations calculated by use of the amplitude data at the first GPS frequency F1. Curves 2–4 in Figure 2, right panel, indicate the results of estimating the refraction attenuation by use of equation (9) from the phase excess data at the frequencies F2 and F1 (curve 3 and 4, respectively) and the phase excess data F0 obtained after ionospheric correction. For calculation of the refraction attenuation from the phase excess data, coefficient m in equation (9) has been evaluated using the satellites orbital data, which include the position and velocities of the GPS and LEO satellites relative to the center of spherical symmetry, point O (Figure 1). Smooth curves 5 describe results of modeling of the refraction attenuation. Good correspondence between the refraction attenuations obtained from the amplitude and phase data is seen in Figure 2, right panel (curves 1–4). Also, results of modeling of the refraction attenuation coincide well with experimental data. Thus, we may conclude that relationship (9) is valid in the RO experiments up to altitudes about 30–40 km.

[21] The relationship (9) opens a new way to measure the refraction attenuation in different kinds of RO experiments including the investigation of the planetary atmospheres. Thus, the phase acceleration has the same importance for the RO experiments as the well-known Doppler frequency. Note that by use of the phase data, one can correct the amplitude data for systematic errors caused by the trends in the antenna gain and direction and receiver's noise variations.

[22] In the following we will consider a possibility to locate the tangent point T on the ray GTL (Figure 1) by use of equations (13), (14) and (15). When RO beam moves through the lower stratosphere and troposphere, the tangent point T is nearly coincides with projection Q of the center of the spherical symmetry, point O on the line of sight GL (Figure 1). In the mesosphere and upper stratosphere, the vertical gradients corresponding to influence of neutral gas are weak and the tangent point T may be displaced because of the influence of the inclined plasma layers in the E or F layers of the ionosphere [*Wickert et al.*, 2004a]. In this case, the center of local spherical symmetry is displaced to point O' and its projection to the line of sight will be disposed at point Q' (Figure 1). New location of the tangent point will coincide with point T' at the distance D from ray perigee T (Figure 1). There exists a possibility to determine the distance D as a difference between the distance $Q'L$ and QL. The distance QL can be determined from the satellites orbital data. The distance $Q'L$ can be found from equation (8) by use of parameter m.

[23] To check a possibility of measuring the distance D, we will consider the CHAMP data relevant to two equatorial RO events 0136 (14 January 2003, at 14 h 40 min local time at the geographical coordinate 3.2S latitude and 3.8E longitude) and 0023 (21 September 2003, at 17 h 52 min local time at the geographical coordinate 6.3S latitude and 139.4W longitude), which are shown in Figure 3 for the 10- to 40-km (left panel) and 5- to 40-km (right panel) height interval, respectively. The phase acceleration a calculated as the second temporal derivative of the phase-path excess and intensity variations $X - 1$ at the frequency F1 are shown in Figure 3 (curves 1 and 2, respectively). As seen in Figure 3, there is a good correspondence between variations of the phase acceleration and intensity of the RO signal. Coefficient m is different in the RO events no. 0136 and no. 0023. Average ratio of the refraction attenuation and the phase acceleration m is about 1.0 s^2/m in the 5- to 40-km height interval for RO event 0136. This value m is about 1.5 times greater than that for RO event 0136. Curve 3 in Figure 3

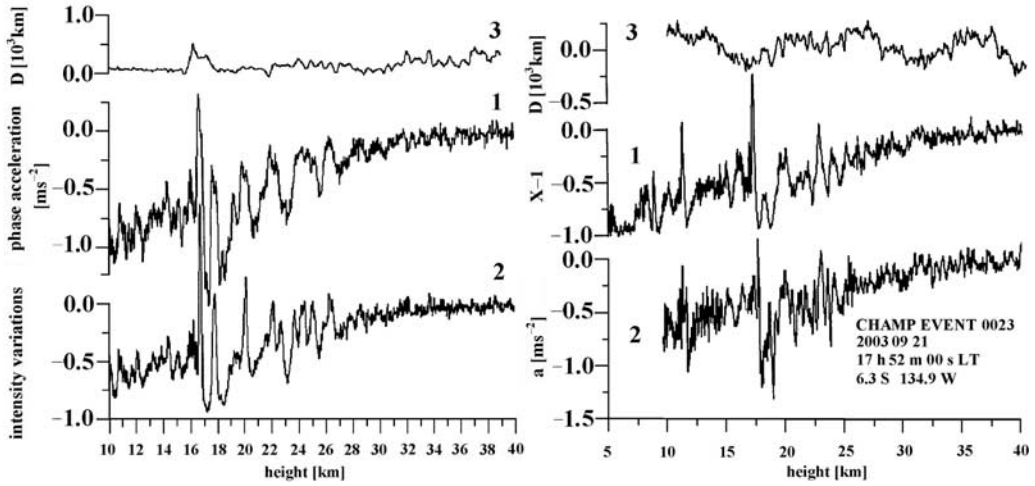

Figure 3. Phase acceleration a and refraction attenuation $X - 1$ at the first GPS frequency F1 (curves 1 and 2, respectively) for two CHAMP RO events, no. 0136, 14 January 2003 (left panel) and no. 0023, 21 September 2003 (right panel). Below 10-km altitude phase acceleration a was not estimated because high variability of phase data. Curves 3 indicate the altitude dependence of distance D calculated by use of equation (11) with averaging on 129 samples (2.5-s time interval).

indicates the deflection D of point T from its standard location in the atmosphere. Deflections in the direction to point G or to point L are positive or negative, respectively. Deflection of point T in the 10- to 20-km interval of altitude from its standard position is mostly small $\sim\pm$150-km besides 16-km altitude, where the deflection is around 500 km. This indicates the atmospheric origin of the phase and amplitude variations of the RO signal at these altitudes.

[24] A correlation between the refraction attenuation and phase acceleration is clearly seen in the 10- to 30-km altitude interval as shown above. Slow regular changes of the refraction attenuation and phase acceleration introduce main contribution to this correlation. Below 10-km altitude, this correlation is destroyed by multipath propagation of the radio waves in the troposphere. Above 30-km altitudes, the ionospheric effect becomes important. Below we will consider a possibility to use ionospheric effect for locating the ionospheric layers.

[25] Examples of the refraction attenuation recalculated from the amplitude and phase data X_a and X_p are shown in Figure 4 (curves 1 and 2) for CHAMP RO event 0015, 21 September 2003 (left panel) and 0023, 21 September 2003 (right panel). The forms of the refraction attenuations X_a and X_p are similar and indicated ionospheric layers at the altitudes of ray perigee 95 and 80 km (Figure 4, left and right panels, respectively). The width of both ionospheric layers, as estimated from curves 1 and 2 in Figure 4, is about 2 km. Altitude 80 km is unusual for ionospheric layers. Thus, in this case, the center of spherical symmetry is displaced and the altitude of ionospheric layer must be recalculated. Results of estimation of the upper and lower boundaries for displacement D with averaging on 2.5-s time

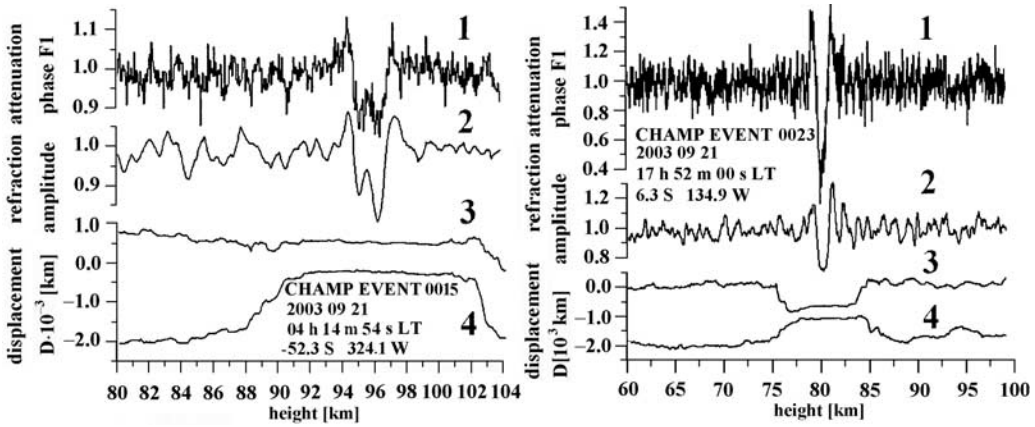

Figure 4. Comparison of the refraction attenuation of the radio waves found from the phase and amplitude data (curves 1 and 2) with results of distance D estimation by use of equations (11) (curve 3) and (12) (curve 4) for CHAMP RO event 0015, 21 September 2003 (coordinate 52.3S, 324.1W, 04 h 14 min 54 s LT) (left panel) and 0023, 21 September 2003 (coordinate 6.3S, 134.9W, 17 h 52 min 00 s LT) (right panel).

Table 1. Displacement D and Correction Δh in the Height of Tangent Point

Height h, km	Distance D, km	$\Delta h = d^2 / 2r$, km	Refraction Attenuation (F1 Phase Data) X_p	Refraction Attenuation (F1 Amplitude data) X_a	Ratio m Refraction Attenuation/ Phase Acceleration Variations, s^2/m
95.746	52.9	0.21	0.8987	0.8956	0.3762
95.700	9.3	0.00	0.9010	0.9000	0.3685
95.655	−26.5	0.05	0.9031	0.9038	0.3621
95.610	61.5	0.29	0.9096	0.9065	0.3776
95.564	8.6	0.00	0.9094	0.9086	0.3683
95.519	−121.7	1.15	0.9051	0.9102	0.3452
95.474	43.5	0.14	0.9145	0.9122	0.3744
95.428	28.9	0.06	0.9143	0.9127	0.3718
95.383	−121.5	1.15	0.9098	0.9146	0.3452
95.338	−14.5	0.01	0.9152	0.9154	0.3641
95.292	47.0	0.17	0.9201	0.9179	0.3749
95.247	−105.4	0.86	0.9179	0.9216	0.3480
95.201	−59.2	0.27	0.9239	0.9256	0.3561
95.156	64.9	0.32	0.9323	0.9298	0.3780
95.111	−179.1	2.50	0.9317	0.9373	0.3349
95.065	−33.8	0.08	0.9428	0.9434	0.3605

interval (M = 64 samples) are indicated by curves 3 and 4, correspondingly, for CHAMP RO events 0015 (Figure 4, left panel) and 0023 (Figure 4, right panel). For event 0015, the upper and lower boundaries for displacement D near altitude 95 km are about 450 and −500 km (curves 3 and 4, respectively, Figure 4, left panel).

[26] One can estimate displacement D and parameter m by use of equations (13), (14), and (15) near the center of layer at altitude h equal to 95 km (Figure 4, left panel). Results of determination of parameter m, displacement D, and correction to the layer altitude Δh are given in Table 1 as function of altitude h of ray perigee T. Also, the refraction attenuations X_a, estimated from amplitude data, and refraction attenuation X_p calculated from equation(6) by use of the measured phase acceleration a and estimated value of parameter m are given in Table 1. The refraction attenuations X_a and X_p are nearly equal, thus indicating the small magnitude of displacement D. The displacement D as seen from the second column of Table 1 is changing in the −180-km to +65-km interval and corresponding corrections to the altitude Δh are about 0.3 km in average. Therefore results of estimation of parameter m by use of equation (13) confirm location of sporadic E layer at the height 95.5 km with small displacement $D \sim -30$ km from ray perigee T (Figure 1). One can estimate by use of data in Table 1 the influence of random errors on the evaluation of distance D from equation (13). Parameter m (Table 1, last column) changes in the 0.3349−0.3780 s^2/m interval with statistical error ± 0.028 s^2/m and relative error ±.8.1%. The estimated distance D (Table 1, second column) changes in the −179.1- to 64.9-km interval with statistical error ±65 km. The accuracy in the evaluation of distance D by considered technique corresponds to theoretical limit of horizontal resolution of RO method estimated previously as ±100 km. It follows that estimation of parameter m from equation (13) is more precise than from equations (14) and (15) in the case of strong scintillations of the amplitude and phase caused by layered structures in the ionosphere.

[27] Altitude 80 km observed in the event 0023 (Figure 5, right panel, curves 1 and 2) is unusual for sporadic ionospheric layer. Thus, in this case, the center of spherical symmetry is displaced and the altitude of ionospheric layer must be recalculated. The large difference (about two times) between the refraction attenuations X_a and X_p calculated from the amplitude and phase data under the assumption of the spherical symmetry with the center at point O (Figure 1) (curves 1 and 2 in Figure 4, right panel) supports this conclusion. Curves 3 and 4 (Figure 4, right panel) indicate the displacement D in the interval from −600 km (upper boundary) to −900 km (lower boundary). A more careful investigation by use of equation (13) gives value D in the −680- to −630-km interval, and correction to altitude Δh is about 30 km. Thus the real height of sporadic E layer is about 110 km. The layer is displaced by 650 km to receiver from the ray perigee T (Figure 1) and has inclination $\delta \approx 6$ to the local horizontal direction. The height of sporadic E layer is increased in the receiver direction. The lower boundary of the horizontal length of sporadic E layer L_e can be estimated from relationship $L_e \approx \Delta d / \delta$ where Δd is the layer width estimated on the dependence of the refraction attenuation on height. For event 0023 (Figure 4, right panel), value $\Delta d \approx 3.5$ km and the horizontal length of E layer is greater than 35 km.

[28] Another example of intensive sporadic E layer is given in Figure 5, left panel (CHAMP RO event 0034, 21 September 2003, 05 h 11 min 13 s LT, 19.9N 227.9W). Curves 1 and 2 (Figure 5, left panel) indicate the refraction attenuations X_a and X_p, respectively, as the functions of altitude h of ray perigee T (Figure 1). Curves 3 and 4 demonstrate the upper and lower boundaries, respectively, for displacement D (Figure 5, left panel). As seen in Figure 5 (left panel), both minima in the refraction attenuations found from the amplitude and phase data correspond to height $h \approx 100$ km. The upper and lower boundaries of the displacement D are nearly coinciding and equal to 500 km (curves 3 and 4, Figure 5, left panel). This value D corresponds to location of the tangent point T' in sporadic E layer between transmitter G and ray perigee T (Figure 1) at altitude $h + \Delta h$ where $\Delta h \approx 18$ km. By use of theoretical relationships published by *Liou et al.* [2006], it is possible to retrieve the variations of the electron density $dN_e(h)$ and its gradient $dN_e(h) / dh$ from the variations of the refraction attenuation, indicated by curves 1 and 2 in Figure 5. Restored variations of the electron density $dN_e(h)$ and its gradient $dN_e(h)/dh$ are shown in Figure 5, right panel, by curves 3 and 4, respectively. The electron density variations

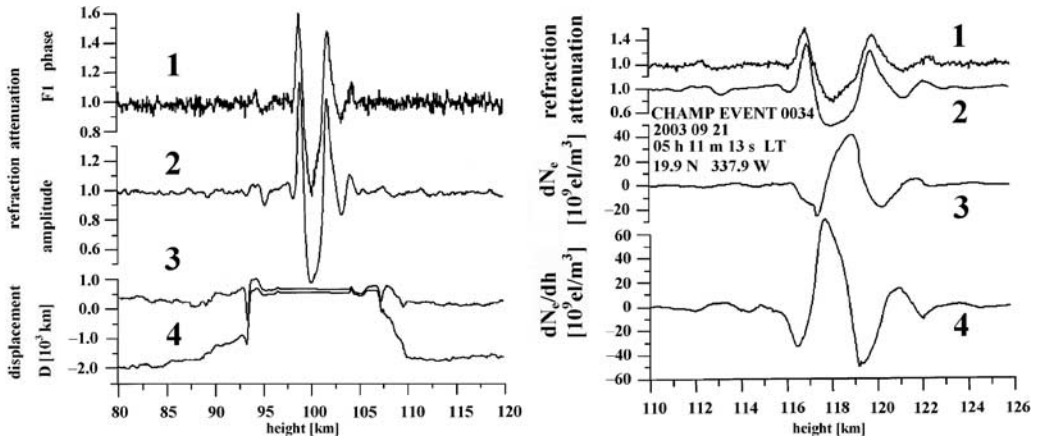

Figure 5. Left panel, comparison of the refraction attenuation of the radio waves found from the phase and amplitude data (curves 1 and 2) with results of distance D estimation by use of equations (13) (curve 3) and (14) (curve 4) for the CHAMP RO event 0034, 21 September 2003 (coordinate 19.9N 227.9W, 05 h 11 min 13 s LT) as function of the altitude of the ray perigee T h. The time interval for averaging was equal to 2.5 s, $M = 64$ samples. Right panel, comparison of the refraction attenuation of the radio waves found from the phase and amplitude data (curves 1 and 2) with results of estimation of the electron density and its vertical gradient variations (curves 3 and 4) as function of the real altitude of the sporadic E layer $h + \Delta h$.

are concentrated at altitudes 116–120 km in the interval ±30 [$10^9 m^{-3}$], and the vertical gradient of the electron density changes in the ±60 [$10^9 m^{-3} km^{-1}$] interval. Maximum in the electron density variation is about of 40 [$10^9 m^{-3}$] and is displaced by 1.5 km relative to minimum of the refraction attenuation disposed at 118-km altitude. Maximum in the vertical gradient of the electron density is about 70 [10^9 $m^{-3} km^{-1}$] and locates by 0.5 km below relative to minimum of the refraction attenuation. Additional example of application of the phase acceleration/intensity ratio technique to analysis of the amplitude and phase variations is given in Figure 6.

[29] Sporadic E layer contributions to variations of the RO signal are considered in detail in Figure 6 (left panel) for CHAMP RO event 0169, 05 July 2003, 29.4S 232.9W. The displacement can be estimated by using curves 3 and 4 (Figure 6, left panel). The centre of sporadic E layer is located at 119.5-km altitude and practically coincide with the RO ray perigee since the distance d (curve 3 and 4 in Figure 6, left panel) is equal to 0. The accuracy in the determination of value d, which may be estimated as a difference between curves 3 and 4 in Figure 3, is about 30–100 km. Results of restoration of the electron density variations $dN_e(h)$ and its gradient $dN_e(h)$ / dh from the amplitude variations of the RO signal are given for the

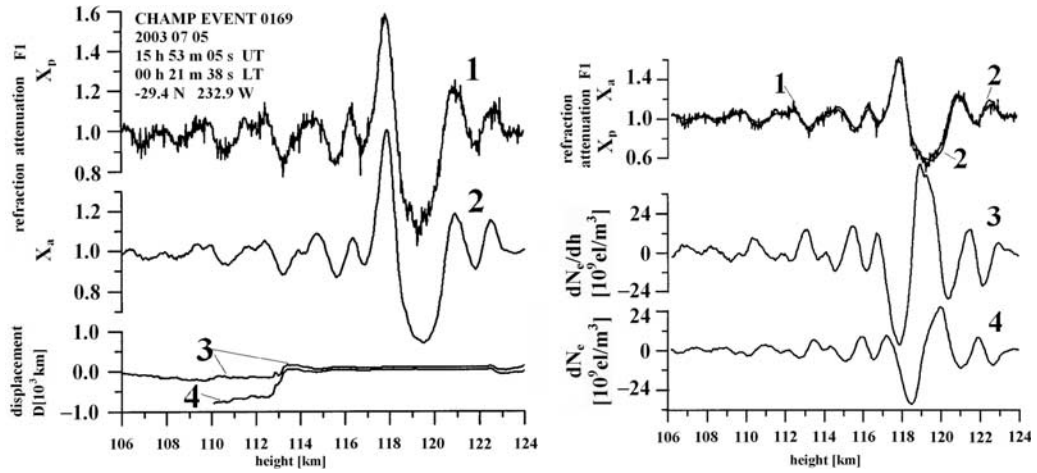

Figure 6. Left panel, comparison of the refraction attenuations X_a and X_p retrieved from the amplitude and phase variations at the first GPS frequency F1 (curve 1 and 2) and results of determination of the displacement of point T from the RO ray perigee (curves 3 and 4) for CHAMP RO event 0169, 5 July 2003, 29.4S 232.9W. Right panel, the refraction attenuations X_a and X_p retrieved from the amplitude and phase variations at the first GPS frequency F1 (curve 1 and 2) and retrieved variations of the electron density and its vertical gradient as functions of the corrected height in the ionosphere for CHAMP RO event 0169.

considered RO event 0169 in Figure 6 (right panel). The initial data, phase acceleration a and refraction attenuation $X - 1$, are shown by curves 1 and 2 in Figure 6 (right panel). Curves 3 and 4 in Figure 4 demonstrate the retrieved variations $dN_e(h)$ and $dN_e(h)$ / dh as functions of the corrected height h. Both curves 1 and 2 are nearly coinciding (Figure 6, right panel). This is a new validation of the equation (6) for the case of sporadic E layers in the ionosphere. The electron density perturbations $dN_e(h)$-changes mainly in the $\pm 5 \times 10^9$ to $\pm 25 \times 10^9$ m^{-3} interval, and its vertical gradient $dN_e(h)$ / dh in the $\pm 20 \times 10^9$ to $\pm 50 \times 10^9$ m^{-3} km^{-1} interval. The estimated heights and plasma parameters are usual values for the sporadic E layer in the ionosphere [e.g., *Kelley*, 1989]. Therefore the suggested method has a promise to be an effective tool for the localization of the sporadic E layers and inclined plasma layers in the ionosphere.

4. Variations of the S_4 Index and Solar Activity

[30] As stated above, the amplitude scintillations are very important because in the case of layered structures, they are directly connected from one side with the phase acceleration and from another side with the vertical gradients of refractivity in the plasma layers. The emphasis in the RO studies is now concentrating on the phase variations of the RO signals in the trans-ionospheric links because direct connection with total electron content [*Hocke and Tsuda*, 2001; *Hocke et al.*, 2001, 2002; *Wickert et al.*, 2004b] and on analysis of the amplitude variations owing to their dependence on the vertical gradient of refractivity [*Vorob'ev et al.*, 1999; *Igarashi et al.*, 2001, 2002; *Gorbunov et al.*, 2002; *Sokolovskiy et al.*, 2002; *Pavelyev et al.*, 2002, 2003, 2005a; *Liou et al.*, 2002, 2003, 2005]. However, the statistical analysis of the amplitude variations of the RO signals, having different origin, is now in the beginning stage. *Wickert et al.*, [2004a, 2004b], *Pavelyev et al.*, [2005b], and *Wu et al.*, [2005] directed special attention toward the amplitude and phase variations caused by sporadic E_s layers in the ionosphere and excluded from analysis the amplitude and phase variations caused by the other factors. *Wickert et al.* [2004a, 2004b] and *Pavelyev et al.* [2005b] considered the amplitude variations as a general characteristic of the ionospheric influence on the RO signal. They concluded that (1) the S_4 index of amplitude variations can be considered as an index of the ionospheric plasma influence on the RO signal in the trans-ionospheric satellite-to-satellite links in a like fashion with the S_4 index introduced formerly for the trans-ionospheric satellite-to-Earth links [e.g., *Yeh and Liu*, 1982]; (2) the S_4 index can be used in the satellite-to-satellite links as a radio-physical index of activity of plasma disturbances in the ionosphere; and (3) the relative number of GPS RO events with high values of the S_4 index in the satellite-to-satellite links can be used to establish a connection between the intensity of plasma disturbances and solar activity.

[31] Below we will follow the point of view introduced by *Wickert et al.* [2004a] and *Pavelyev et al.* [2005b] for the analysis of the influence of the ionospheric plasma on the RO signal and revealing connections of the amplitude variations with solar activity. We will describe the amplitude variations of the RO signal by the magnitude of the S_4 scintillation index [e.g., *Yeh and Liu*, 1982; *Aarons*, 1982]:

$$S_4 = \left[< (I - < I >)^2 > \right]^{1/2} / < I >, \qquad (16)$$

where $<>$ is the average relevant to the height $h(T)$ above 40 km, and $I(t)$ is the intensity of the RO signal. When the amplitude and phase variations are caused by layered ionospheric structures, the S_4 scintillation index can be connected with the refraction attenuation $X - 1$ and the phase acceleration variations a [equation (6)]:

$$S_4 = \left[< (X - 1)^2 > \right]^{1/2} = m \left[< a^2 > \right]^{1/2}. \qquad (17)$$

[32] The relationships (6) and (14) give new possibility to reveal the origin of the phase and amplitude scintillations in the near-Earth propagation medium and may have a general significance for the trans-ionospheric satellite-to-satellite and satellite-to-Earth links. In the following we will indicate that the S_4 scintillation index is a key parameter connecting the amplitude variations of the RO signal with space weather conditions on a global scale.

[33] Influence of sporadic solar activity can be considered in the case of solar flare during 29–31 October 2003. To analyze in more details the geographic and time distributions of the amplitude scintillations in the RO signal, we treat about 2000 CHAMP RO events from 27 October to 9 November 2003. The histograms of the integral distribution of the S_4 index, which have been obtained for each day of measurements, are shown in Figure 7. The ratio R_i of the number of cases with the magnitude S_4 larger than the value plotted on the abscissa to the total number of measurements for the corresponding day is plotted on the ordinates in Figure 7. The histograms in the right-hand panel of Figure 7 correspond to data of S_4 measurements on 29–31 October, as well as on 28 October, 1 November, and 4 November 2003, performed during relatively intense and weak disturbances in the RO signal, respectively. The initial histogram values for the entire period of observations are coincident and correspond to an amplitude S_4 of ~2.8%, which depends on the level of fluctuations of receiver noise. Three days, 29–31 October, with considerably higher S_4 levels than on the remaining days are distinguished in Figure 7.

[34] The most difference between the histograms is observed in the 5–19% interval of the S_4 index with maximum of about 12% (Figure 7, left and right panels). The value 12% of the S_4 index is by a factor 4.3 greater than the level of the receiver's noise. Therefore, in the CHAMP RO experiments at the first GPS frequency, the values of S_4 index in the 5–19% interval can be considered as the most sensitive for estimation of the ionospheric influence on the RO signal. An analysis performed makes it possible to introduce the RO index of ionospheric activity R_i.

[35] By definition, the R_i index is equal to the ratio of the number of RO events with the S_4 value of the RO signal at $h > 40$ km larger than 3–4 magnitudes of S_4 caused by technical noise of the transmitter-receiver system to the total number of RO events for a certain time interval (for example, for a day). The R_i variations for the

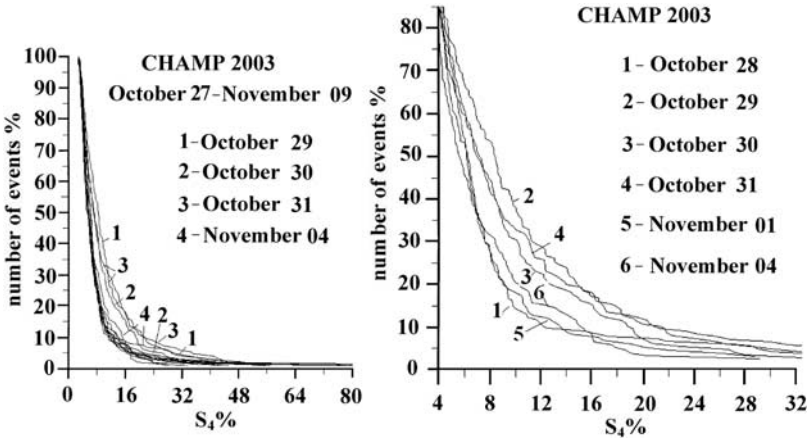

Figure 7. Histograms of the S_4 index variations corresponding to perigee altitudes of the CHAMP RO signal trajectory (point *T*in Figure 1) higher than 40 km. The curves corresponding to the histograms for 27 and 28 October and for 1–3 and 5–9 November 2003 are almost indiscernible in the left-hand panel. The right-hand panel demonstrates the histograms (curves 1–6) in more details.

period from 27 October to 9 November 2003 are shown in Figure 8 (left-hand panel). The histograms in Figures 6 and 7 (left-hand panel) are in good agreement with the variations in the hourly index of the solar wind magnetic field (*DST*, nT) obtained from data of the satellite measurements. During 26–28 October, 1–3 November, and 5–9 November, the *DST* index was almost constant, which corresponds to decreased values of the integrated distributions in the histograms (Figure 7 and Figure 8, left-hand panel). Abrupt changes in the index of the solar wind magnetic field were observed on 29–31 October and 4 November, which corresponds to a twofold increase in the number of events with increased (larger than 12%) S_4 index of the variations in the RO signal intensity (Figure 8, left-hand panel).

[36] The geographic distributions of increased (greater than 12%) S_4 index of the variations in the RO signal amplitude on 26–28 October (right panel) and on 29–31 October 2003 (left panel) are compared in Figure 9. According to Figure 9, the general number of events with S_4 index values greater than 12% increased by 2.5 times in period 29–31 October as compared with period 26–28 October. The most important changes occurred mainly in the Polar Regions in Antarctica and in the Northern Hemisphere near geomagnetic South and North poles. It is interesting to note that ionospheric disturbances (Figure 9, left and right panels) are concentrated above continents near coasts and in mountain regions (eastern coast of Asia, Japan, Kamchatka, western regions of South America, etc.). This corresponds to observations made previously by *Hocke et al.* [2001].

5. Geographical and Seasonal Distributions of CHAMP RO Events With Intense Amplitude Variations

[37] The geographical distributions of the intense ionospheric events (with the S_4 index greater than 0.12) for all

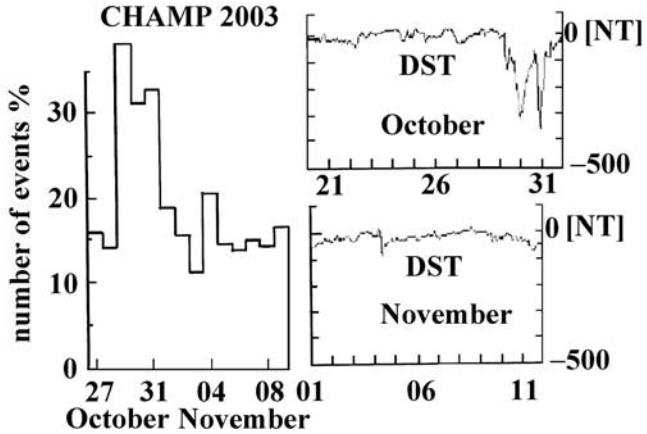

Figure 8. Left-hand panel, the histogram of the RO events with S_4 index higher than 5% according to data of the CHAMP measurements performed from 27 October to 9 November 2003. Right-hand panel, the dynamics of the hourly index of the solar wind (*DST*, nT) according to data from http://swdcwww.kugi.kyoto-u.ac.jp/aeasy/index.html for 26–31 October (upper part of the right panel) and 1–11 November 2003 (bottom part of the right panel).

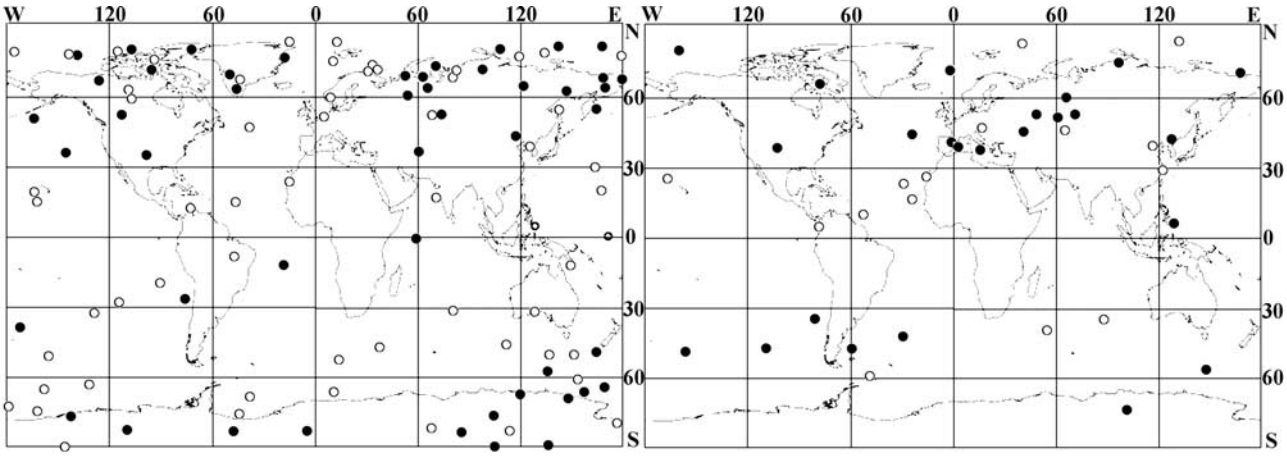

Figure 9. The geographic distribution of the RO events with S_4 index value higher than 12% on 26–28 October 2003 (right panel) and 29–31 October 2003 (left panel). Open and solid circles correspond to the nighttime (from 2000 to 0800 LT) and daytime (from 0800 to 2000 LT) local time intervals, respectively.

types of the amplitude scintillations in the CHAMP RO signals at 1575.42 MHz are demonstrated in Figures 10 and 11. Note, that these distributions may be linked to changes in sampling by CHAMP. Our analysis showed that the satellite coverage over the relevant periods was nearly regularly distributed. Therefore these distributions contain important information on the spatial dependence of the strong ionospheric events during the considered time intervals. The distributions of the ionospheric events indicate that they are concentrated in some regions (for example, the equatorial and geomagnetic North and South polar zones in Figures 10 and 11). High activity in some equatorial regions may be connected with the evening ionospheric disturbances that arise after sunset, 20–24 hours local time, in

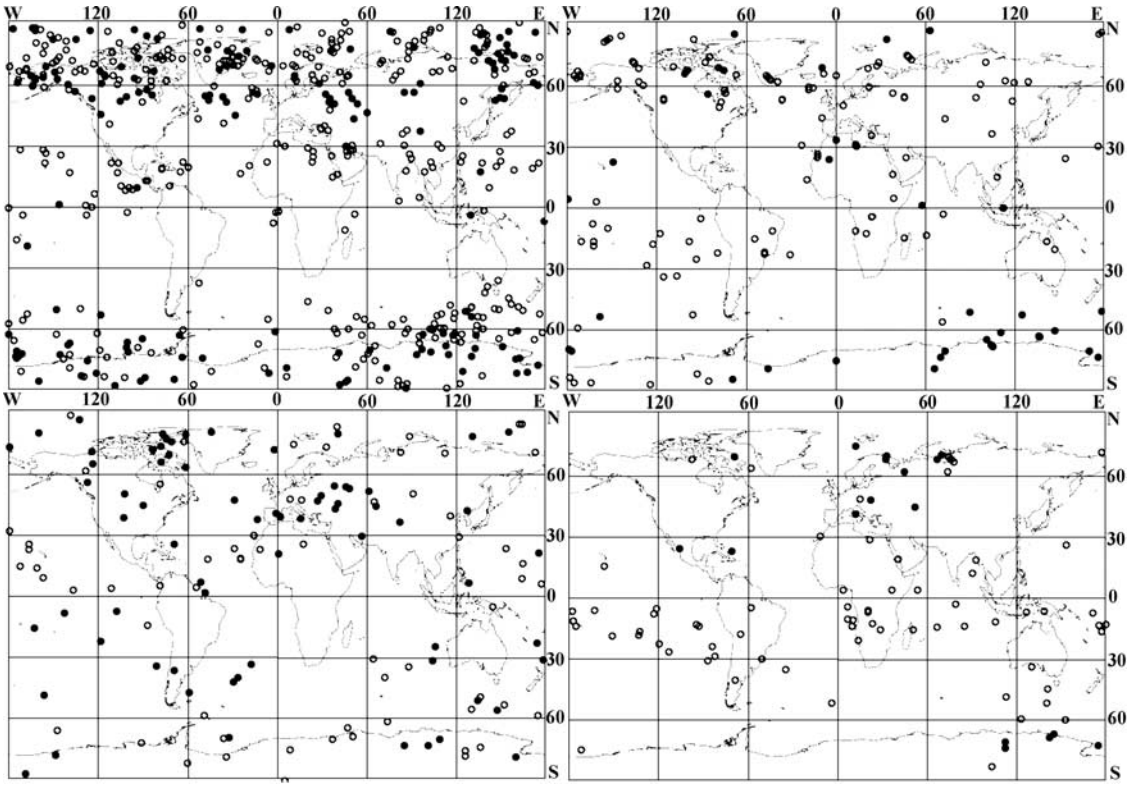

Figure 10. Maps of intense ionospheric events with S_4 index greater than 0.12 for October 2001 (left top panel), October 2002 (right top panel), October 2003 (left bottom panel), and April 2004 (right bottom panel). The circles show the geographical position of the tangent point T (Figure 1). The daytime events are marked by closed circles (local time 08–20 hours) and the nighttime events are indicated by open circles (local time 20–08 hours).

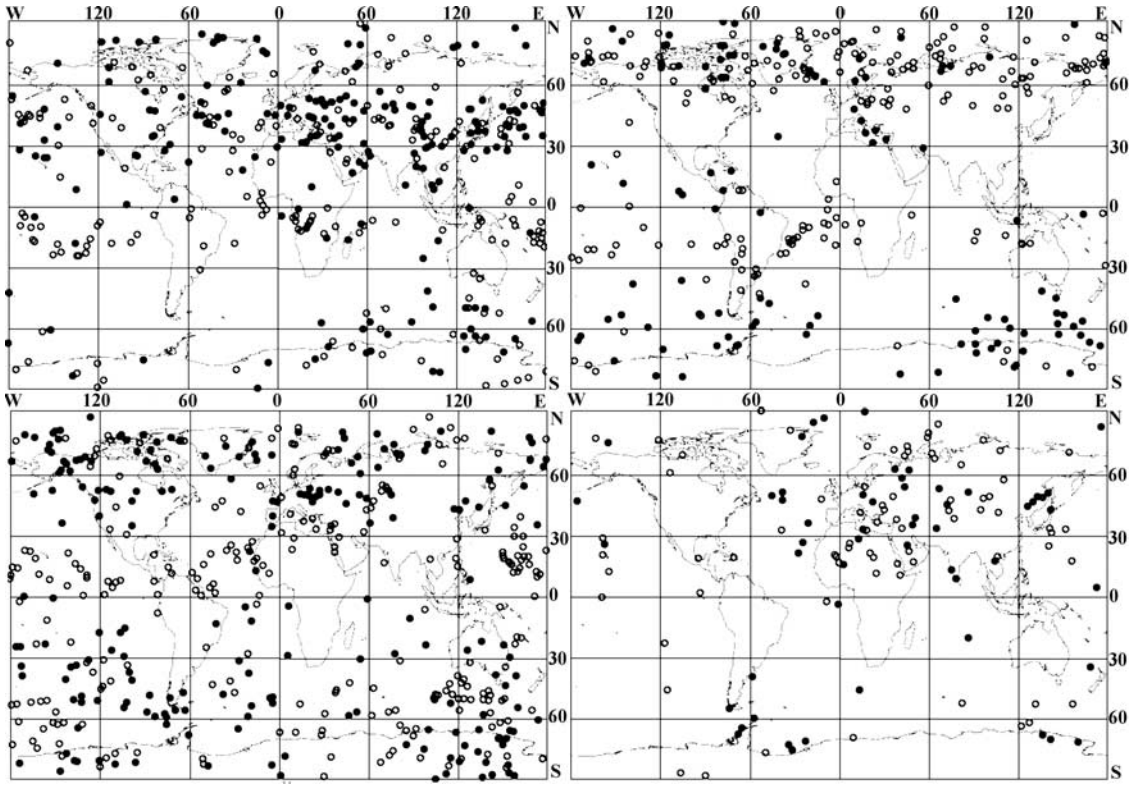

Figure 11. Seasonal dependence of the global distribution of CHAMP RO events with intense amplitude variations (with magnitude of S_4 index greater than 0.2) for periods 14 May to 14 July 2001 (left top panel), November to December 2001 (right top panel), 28 October to 26 November 2003 (left bottom panel), July 2004 (right bottom panel). The daytime events are marked by closed circles (local time 08–20 hours), the nighttime events are indicated by open circles (local time 20–08 hours).

accordance with the Earth-based measurements reviewed earlier [e.g., *Yeh and Liu*, 1982]. Note that geographical distributions of the nighttime and daytime events are very different. The daytime events prevail in the North and South Polar zones. The nighttime events are concentrated mainly in the equatorial and moderate latitude areas. The most significant difference in the geographical distributions of nighttime (open circles) and daytime (closed circles) events is observed in April 2004 (Figure 11, right bottom panel) and in October 2002 (Figure 10, right top panel). This indicates the different origin of the daytime and nighttime plasma disturbances in the ionosphere. The number and geographical distributions of intense ionospheric events depend on time.

[38] The maximal number of events can be seen in May–July, October–December 2001 (Figure 10, left top panel, Figure 11, left and right top panels, respectively). The minimal number of events corresponds to October 2002 (right top panel in Figure 10) and April and July 2004 (bottom right panels in Figures 10 and 11, respectively). As seen in Figures 10 and 11, the number of intense ionospheric events and their intensity decreases as time from May, July, and October 2001 to April–July 2004. This is possibly connected with a gradual diminishing in solar activity from maximal values in 2001 to minimal values in 2004.

[39] One can estimate the seasonal dependence in the geographical distributions of intense ionospheric events registered by the CHAMP satellite (Figure 11). The seasonal displacement of the regions with intense ionospheric events in the south and north directions during the periods from May–July 2001 (Figure 11, left top panel) to November–December 2001 (Figure 11, right top panel) and to September 2001 (Figure 10, left top panel) can be noted. The number of intense ionospheric events increases in the North Polar Region with latitudes greater than 60N as the time changes from May–July 2001 to November–December 2001. Also, the number of intense ionospheric events decreases at the moderate latitudes in the 30–60N interval for the same time interval. The possible cause of the seasonal dependence may be connected with two important mechanisms governing the ionospheric disturbances. The first one is the ionizations caused by energetic electrons in the Polar Regions; the second is due to solar radiation. The influence of solar radiation has a seasonal character because ionization in the ionosphere follows annual and diurnal motion of the ionospheric subsolar point. As follows from this consideration, the amplitude part of the RO radio holograms is appropriate for studying the geographical and seasonal distributions of the ionospheric disturbances with global coverage and establishing their connections with solar activity.

6. Conclusions

[40] As a result of the study, we show that the RO signal variations are an indicator of plasma disturbances in the near-Earth space. The correlated phase acceleration and intensity variations of the RO signal are mainly affected

by inclined ionospheric layers where an intensive electron density gradient is perpendicular to a radio wave propagation trajectory. The phase acceleration/intensity ratio technique is a new method for locating the inclined layered structures (including sporadic E_s layers) in the ionosphere. This method is validated by measuring the location of the tangent points in the atmosphere and ionosphere by means of analysis of the CHAMP RO data. The new phase acceleration/intensity ratio technique gives the quantitative connection between the phase variations and amplitude variations and allows establishing the origin of scintillation of radio signals in the trans-ionospheric satellite-to-satellite and satellite-to-Earth links.

[41] An analysis of the histograms of the RO signal amplitude variations corresponding to the solar event 29–31 October 2003 indicates a possibility to introduce the RO index of ionospheric activity R_i, which is in good agreement with changes in the hourly index of *DST* related to the solar wind. This index can be introduced on the basis of the well-known index S_4, which is widely used as a measure of the amplitude of scintillations in the trans-ionospheric satellite-to-Earth links. The R_i index is equal to the ratio of the number of the RO events with the S_4 value, averaged at the altitudes above 40 km, and greater than the selected level, to the total number of RO events in the investigated area for a certain time interval (for example, for a day). The maps of the geographical and seasonal distribution of the intense RO amplitude scintillations with high values of the index S_4, relevant to the time period May 2001 to July 2004, indicate the areas with intense ionospheric disturbances and demonstrate the connection with solar activity.

[42] The analysis indicates the importance of GPS RO studies for revealing the interrelations between solar activity and natural processes in the ionosphere and mesosphere.

[43] **Acknowledgments.** We are grateful to the Center of Geophysical Studies, Potsdam, for CHAMP experimental data on radio occultation. The work has been partly supported by National Science Council of Taiwan (NSC) grant NSC 94-2811-M-008-055, Russian Foundation for Basic Researches grant no. 06-02-17071, and programs OFN-16, OFN-17 Russian Academy of Sciences (RAS). We are thankful to the anonymous Referees for their constructive remarks and comments, which help us to improve our paper.

[44] Amitava Bhattacharjee thanks the reviewers for their assistance in evaluating this paper.

References

Aarons, J. (1982), Global morphology of ionospheric scintillations, *Proc. IEEE*, *70*, 360–378.

Gorbunov, M. E., A. S. Gurvich, and A. V. Shmakov (2002), Back-propagation and radio-holographic methods for investigation of sporadic ionospheric E-layers from Microlab-1 data, *J. Int. Remote Sens.*, *23*(4), 675–685.

Hajj, G. A., and L. J. Romans (1998), Ionospheric electron density profiles obtained with the global positioning system: Results from the GPS/MET experiment, *Radio Sci.*, *33*, 175–190.

Hajj, A., E. R. Kursinski, L. J. Romans, W. I. Bertiger, and S. S. Leroy (2002), A technical description of atmospheric sounding by GPS occultation, *J. Atmos. Sol.-Terr. Phys.*, *64*, 451–469.

Heise, S., N. Jakowski, A. Wehrenpfennig, C. H. Reigber, and H. Lühr (2002), Sounding of the Topside Ionosphere/Plasmasphere Based on GPS Measurements from CHAMP: Initial Results, *Geophys. Res. Lett.*, *29*(14), 1699, doi:10.1029/2002GL014738.

Hocke, K., and T. Tsuda (2001), Gravity waves and ionospheric irregularities over tropical convection zones observed by GPS/MET radio occultation, *Geophys. Res. Lett.*, *28*, 2815–2818.

Hocke, K., A. G. Pavelyev, K. Igarashi, et al. (2001), Global sounding of sporadic E layers by the GPS/MET radio occultation experiment, *J. Atmos. Sol.-Terr. Phys.*, *63*, 1973–1980.

Hocke, K., K. Igarashi, and A. Pavelyev (2002), Irregularities of the topside ionosphere observed by GPS/MET radio occultation, *Radio Sci.*, *37*(6), 1101, doi:10.1029/2001RS002599.

Igarashi, K., A. Pavelyev, K. Hocke, D. Pavelyev, and J. Wickert (2001), Observation of wave structures in the upper atmosphere by means of radio holographic analysis of the radio occultation data, *Adv. Space Res.*, *27*(6–7), 1321–1327.

Igarashi, K., A. Pavelyev, J. Wickert, K. Hocke, and D. Pavelyev (2002), Application of radio holographic method for observation of altitude variations of the electron density in the mesosphere/lower thermosphere using GPS/MET radio occultation data, *J. Atmos. Sol.-Terr. Phys.*, *64*, 959–969.

Kelley, M. C. (1989), *The Earth's Ionosphere*, Int. Geophys. Ser., vol. 43, Elsevier, New York.

Kelley, M. C., V. K. Wong, G. A. Hajj, and A. J. Mannucci (2004), On measuring the off-equatorial conductivity before and during convective ionospheric storms, *Geophys. Res. Lett.*, *31*, L17805, doi:10.1029/2004GL020423.

Kunitsyn, V. E., and Tereshchenko (2003), Ionospheric Tomography Springer Verlag Series: Physics of Earth and Space Environments XII, 260 p. 88 illus. ISBN: 3-540-00404-1.

Liou, Y.-A., A. G. Pavelyev, C.-Y. Huang, K. Igarashi, and K. Hocke (2002), Simultaneous observation of the vertical gradients of refractivity in the atmosphere and electron density in the lower ionosphere by radio occultation amplitude method, *Geophys. Res. Lett.*, *29*(19), 1937, doi:10.1029/2002GL015155.

Liou, Y.-A., A. G. Pavelyev, C.-Y. Huang, K. Igarashi, K. Hocke, and S. K. Yan (2003), Analytic method for observation of the GW using RO data, *Geophys. Res. Lett.*, *30*(20), 2021, doi:10.1029/2003GL017818.

Liou, Y. A., A. G. Pavelyev, J. Wickert, T. Schmidt, and A. A. Pavelyev (2005), Analysis of atmospheric and ionospheric structures using the GPS/MET and CHAMP radio occultation database: A methodological review, *GPS Solutions*, *9*(2), 122–143.

Liou, Y. A., A. G. Pavelyev, J. Wickert, S. F. Liu, A. A. Pavelyev, T. Schmidt, and K. Igarashi (2006), Application of GPS radio occultation method for observation of the internal waves in the atmosphere, *J. Geophys. Res.*, *111*, D06104, doi:10.1029/2005JD005823.

Pavelyev, A. G., A. V. Volkov, A. I. Zakharov, S. A. Krytikh, and A. I. Kucherjavenkov (1996), Bistatic radar as a tool for Earth observation using small satellites, Acta Astronautica, V.*39*, No.9-12, p.721–730.

Pavelyev, A., A. I. Zakharov, A. I. Kucherjavenkov, E. P. Molotov, A. I. Sidorenko, I. L. Kucherjavenkova, and D. A. Pavelyev (1997), Propagation of radio waves reflected from Earth's surface at grazing angles between a Low-Orbit Space Station and Geostationary Satellite, *J. Commun. Technol. Electron.*, *42*(1), 45–50.

Pavelyev, A., K. Igarashi, C. Reigber, K. Hocke, J. Wickert, G. Beyerle, S. Matyugov, A. Kucherjavenkov, D. Pavelyev, and O. Yakovlev (2002), First application of radioholographic method to wave observations in the upper atmosphere, *Radio Sci.*, *37*(3), 1043, doi:10.1029/2000RS002501.

Pavelyev, A. G., T. Tsuda, K. Igarashi, Y. A. Liou, and K. Hocke (2003), Wave structures in the electron density profile in the ionospheric D and E-layers observed by radio holography analysis of the GPS/MET radio occultation data, *J. Atmos. Sol.-Terr. Phys.*, *65*(1), 59–70.

Pavelyev, A. G., Y. A. Liou, and J. Wickert (2004), Diffractive vector and scalar integrals for bistatic radio holographic remote sensing, *Radio Sci.*, *39*(4), RS4011, doi:10.1029/2003RS002935.

Pavelyev, A. G., J. Wickert, Y. A. Liou, Ch. Reigber, T. Schmidt, K. Igarashi, A. A. Pavelyev, and S. S. Matyugov (2005a), Different mechanisms of the ionospheric influence on GPS occultation signals, *GPS Solutions*, *V.9*(1), 96–104.

Pavelyev, A. G., J. Wickert, T. Schmidt, Ch. Reigber, S. S. Matyugov, A. A. Pavelyev, Y. A. Liou, and K. Igarashi (2005b), Effect of solar activity in late October 2003 on radio occultation signals from the CHAMP German satellite, *Geomagn. Aeron.*, *45*(1), 134–139.

Schreiner, W. S., S. V. Sokolovskiy, C. Rocken, and D. C. Hunt (1999), Analysis and validation of GPS/MET radio occultation data in the ionosphere, *Radio Sci.*, *34*(4), 949–966.

Sokolovskiy, S., W. Schreiner, C. Rocken, and D. Hunt (2002), Detection of high-altitude ionospheric irregularities with GPS/MET, *Geophys. Res. Lett.*, *29*(3), 1033, doi:10.1029/2001GL013398.

Steiner, A. K., G. Kirchengast, and H. P. Ladreiter (1999), Inversion, error analysis and validation of GPS/MET data, *Ann. Geophys.*, *17*, 122–138.

Vorob'ev, V. V., A. S. Gurvich, V. Kan, S. V. Sokolovskiy, O. V. Fedorova, and A.V. Shmakov (1999), Structure of the Ionosphere from the radio-occultation GPS-"Microlab-1" satellite data: Preliminary results, *Earth Obs. Remote Sens.*, *15*, 609–622.

Yeh, K. C., and C. H. Liu (1982), Radio wave scintillations in the ionosphere, *Proc. IEEE*, *70*(4), 324–360.

Wickert, J., A. G. Pavelyev, Y. A. Liou, T. Schmidt, Ch. Reigber, K. Igarashi, A. A. Pavelyev, and S. Matyugov (2004a), Amplitude variations in GPS signals as a possible indicator of ionospheric structures, *Geophys. Res. Lett.*, *31*(24), 1–4, L24801, doi:10.1029/2004GL020607.

Wickert, J., O. I. Yakovlev, A. G. Pavel'ev, S. S. Matyugov, L. N. Samoznaev, and V. A. Anufriev (2004b), Ionospheric Fluctuations of decimetric radio waves along satellite-to-satellite paths, *J. Commun. Technol. Electron.*, *49*(10), 1109–1116.

Wickert, J., et al. (2001), Atmosphere sounding by GPS radio occultation: First results from CHAMP, *Geophys. Res. Lett.*, *28*(17), 3263–3266.

Wu, D. L., C. O. Ao, G. A. Hajj, M. de la Torre Juarez, and A. J. Mannucci (2005), Sporadic E morphology from GPS-CHAMP radio occultation, *J. Geophys. Res.*, *110*, 1–18, A01306, doi:10.1029/2004JA010701.

Yizengaw, E., M. B. Moldwin, P. L. Dyson, and T. J. Immel (2005), Southern Hemisphere ionosphere and plasmasphere response to the interplanetary shock event of 29–31 October 2003, *J. Geophys. Res.*, *110*, A09S30, doi:10.1029/2004JA010920.

Yizengaw, E., M. B. Moldwin, A. Komjathy, and A. J. Mannucci (2006), Unusual topside ionospheric density response to the November 2003 superstorm, *J. Geophys. Res.*, *111*, A02308, doi:10.1029/2005JA011433.

Y. A. Liou, Center for Space and Remote Sensing Research, National Central University, Chung-Li 320, Taiwan. (yueian@csrsr.ncu.edu.tw.)

S. F. Liu, Department of Industrial Design, National Cheng Kung University, No.1, University Road, Tainan 701, Taiwan. (liusf@mail.ncku.edu.tw)

A. A. Pavelyev and A. G. Pavelyev, Institute of Radio Engineering and Electronics, Russian Academy of Sciences, Fryazino, Vvedenskogo sq. 1, 141190 Moscow Region, Russia. (pvlv@ms.ire.rssi.ru)

T. Schmidt and J. Wickert, GeoForschungsZentrum Potsdam, Telegrafenberg, 14473 Potsdam, Germany. (wickert@gfz-potsdam.de)